J Wood Sci (2006) 52:121–127
DOI 10.1007/s10086-005-0742-7

ORIGINAL ARTICLE

Mariko Yoshioka · Keiji Takabe · Junji Sugiyama
Yoshiyuki Nishio

Newly developed nanocomposites from cellulose acetate/layered silicate/poly(ε-caprolactone): synthesis and morphological characterization

Received: January 11, 2005 / Accepted: May 23, 2005 / Published online: February 5, 2006

Abstract New biodegradable cellulose acetate/layered silicate grafted poly(ε-caprolactone) [(CA/layered silicate)-g-PCL] nanocomposites were prepared by in situ polymerization of ε-caprolactone in the presence of cellulose acetate (CA) and organically modified layered silicate (OMLS). The structures of the resulting composites were investigated. X-ray diffractometry was carried out to survey general structural features of (CA/OMLS)-*g*-PCL nanocomposites, and revealed that OMLSs having hydroxyl groups in the organic modifiers greatly altered the layered silicate structure by monomer intercalation and successive exfoliation through its polymerization. Two of the representative cases were characterized by wide-angle and small-angle X-ray scattering analyses with a synchrotron source. The morphology of these nanocomposites was further examined by transmission electron microscopy. When SPN, one of OMLSs having one hydroxyl group in its modifier, was used, the silicate layers could not be dispersed thoroughly, but existed as aggregates consisting of several silicate layers. Among them, the crystal growth of PCL developed by transcrystallization, where the crystal growth was restricted in the confined space. When Cloisite 30B, having two hydroxyl groups within the modifier, was used, the silicate layers forming the clay were dispersed completely in the composite and random orientation of the OMLS was observed.

Key words Cellulose acetate · Graft copolymerization · Layered silicate · Nanocomposite · Poly(ε-caprolactone)

M. Yoshioka (✉) · K. Takabe · Y. Nishio
Division of Forest and Biomaterials Science, Graduate School of Agriculture, Kyoto University, Kitashirakawa Oiwake-cho, Sakyo-ku, Kyoto 606-8502, Japan
Tel. +81-75-753-6253; Fax +81-75-753-6300
e-mail: mariko@kais.kyoto-u.ac.jp

J. Sugiyama
Research Institute for Sustainable Humanosphere, Kyoto University, Uji 611-0011, Japan

Introduction

Polymer/layered silicate nanocomposites belong to a relatively new class of materials with attractive features, in which nanometer-size silicates, such as montmorillonite and hectorite, are dispersed in the polymeric matrix. These nanocomposites have been produced from various polymers combined with organically modified layered silicates (OMLS), and whether an admixture of polymer and OMLS produces an exfoliated or intercalated nanocomposite depends upon the characteristics of the polymer matrix and the OMLS. These characteristics include the nature of the polymer as well as the type, packing density, and chemical structure of organic modifiers residing in the silicate interlayers. These composite materials can be produced either by melt intercalation or by in situ polymerization. They have unexpected hybrid properties when compared with their microcomposite and macrocomposite counterparts as well as the pure polymer matrix. The physical and mechanical properties have been unexpectedly improved by use of a small amount of layered silicate.[1–22] Because the layered silicates are of mostly natural origin, the polymer/layered silicate nanocomposites can be designed to be environmentally benign when polymers from natural resources are selected. In that sense, poly-L-lactide (PLA) has been recently used as a biodegradable polymer of natural origin.[6,16,17,20] However, there has been almost no attempt to prepare nanocomposites from cellulose-based polymers and layered silicates.

Cellulose-based polymers do not possess melt processability. However, a number of changes, which concern demand for recyclable materials and biodegradable plastics, have recently occurred to provide motivation for both preliminary and ongoing investigations into the conversion of biomass into plastics.[23] During the past few years, authors' groups have attempted to identify novel plasticizing procedures by which biodegradable thermoplastic polymers could be produced from cellulose acetate (CA).[23–26] Among them, especially, in situ graft copolymerization of CA with the use of cyclic esters and tin(II)2-ethylhexanoate

($SnEht_2$) gave excellent results.[23,26] By using this technology, the resultant products can exhibit wide-ranging properties and functionalities caused by the species and combinations of cyclic esters, compositions of introduced graft chains, and so on. It has been reported that CAs with a degree of substitution (DS) of less than 2.5 are biodegradable,[27] and the grafted products described above have biodegradable functionality.

Based on these findings, we have newly prepared (CA/layered silicate)-grafted (g)-poly-ε-caprolactone (PCL) nanocomposites by a dispersion and in situ polymerization technique in order to give higher performance and wide-ranging functions to the grafted cellulose acetates. This study was focused primarily on investigation of morphology for hot-press-molded nanocomposite samples through X-ray diffractometry (XRD) and transmission electron microscopic (TEM) observations. Natural montmorillonite, synthetic hectorite, or synthetic fluoromica modified with several kinds of onium salts were used, respectively, and compared as a filler of nanocomposite.

Experimental

Materials

The clays used and their modifiers are listed in Table 1. Highly purified montmorillonite PGW and I-30T were supplied by Volclay (Japan), Cloisite 30B was purchased from Wilbur-Ellis (Japan), and the remainder were supplied from Co-op Chemical. ε-Caprolactone (CL), and cellulose diacetate (CDA) (DS = 2.2) were supplied by Daicel. Tin (II) 2-ethylhexanoate ($SnEht_2$) was obtained from Wako. Among the above reagents, CL monomer was purified by vacuum distillation before use, but others were used as received.

Methods

Preparation of (CDA/OMLS)-g-PCL nanocomposites

Five grams of vacuum-dried CDA, 20.0 g of CL and 1.25 g of OMLS (5% based on total amounts of CDA and CL) were placed in a four-necked 100-ml flask equipped with a stirrer. Moderate stirring was used at 140°C for 120 min under a nitrogen atmosphere. Then, an amount of $SnEht_2$ corresponding to 1% of the total weight of the components in the flask was added and the reaction was continued at the same temperature for 30 min to obtain (CDA/OMLS)-g-PCL nanocomposites.

Characterization

Gel permeation chromatography (GPC) analysis was carried out for the polymer matrix of nanocomposite products. The molecular weight distribution of the respective samples was determined on a Tosoh HLC-8020 gel permeation chromatograph equipped with a refractive index (RI) detector and using two TSK-GEL GMHHR-H columns connected in series. The analysis was conducted by using tetrahydrofuran (THF) as the mobile phase at a flow rate of 1.0 ml/min. The concentration of the test samples was 0.5% (w/v) in

Table 1. Clays used and their modifiers

Clays used (wt%)	Origins of clays	Modifiers of clays	Hydroxyl groups in modifier
PGW (5)	Highly purified natural montmorillonite	–	–
I-30T (5)	Highly purified natural montmorillonite	Octadecyl ammonium cation	0
Cloisite30B (5)	Highly purified natural montmorillonite	Methyl, tallow (n = 14–18), bis-2-hydroxyethyl, ammonium cation	2
SEN (5)	Synthetic hectorite	Coco-alkyl, dihydroxy polyoxyethyl (m, n = plurals), methyl ammonium cation	2
SPN (5)	Synthetic hectorite	Polyhydroxypropyl (n = 25), diethyl, methyl ammonium cation	1
SAN (5)	Synthetic hectorite	Distearyl, dimethyl, ammonium cation	0
ME-100 (5)	Synthetic fluoromica	–	–
MEE (5)	Synthetic fluoromica	Coco-alkyl (n = 12–14), dihydroxyethyl, methyl ammonium cation	2
MPE (5)	Synthetic fluoromica	Polyhydroxypropyl (n = 25), diethyl, methyl ammonium cation	1
MAE (5)	Synthetic fluoromica	Distearyl, dimethyl, ammonium cation	0

THF and the injection volume was 100 μl. The system was calibrated with monodisperse polystyrene standards.

Sheet-like moldings were prepared from CDA and (CDA/OMLS)-g-PCL nanocomposites by hot pressing at 110°C under 15 MPa gauge pressure for 30 s, and thermoplasticity was examined.

X-ray diffraction (XRD) profiles for PGW, ME-100, OMLS, and (CDA/OMLS)-g-PCL nanocomposites were obtained by using a RINT 2200 V (Rigaku Denki, Tokyo) with Cu Kα radiation (40 kV, 30 mA). Scanning speed and step size were 2° and 0.02°/min, respectively.

Wide-angle X-ray scattering (WAXS) and the small-angle X-ray scattering (SAXS) analyses were performed at BL40XU beam line in SPring-8 facility, Harima, Japan. All the patterns recorded on CCD camera were calibrated either by the diffraction rings from Si or stearic acid standard samples. Most of the data analyses were conducted using the Fit2d program (http://www.esrf.fr/computing/scientific/FIT2D/).

Morphologies of nanocomposites were observed by transmission electron microscopy (TEM). Ultrathin sections about 100 nm thick were cut by a Reichert-Jung Ultracut E microtome equipped with a diamond knife. The images of the clay dispersion in the CDA-grafted PCL matrix polymer was observed under a JEM-1220EX (Jeol, Japan).

Results and discussion

(CDA/OMLS)-g-PCL nanocomposites were prepared by monomer dispersion and polymerization. This involved dispersion of OMLS in CL (organic monomer), dissolving CDA, followed by polymerization of the monomer at a high temperature (140°C) as a mode of intercalating CDA and/or PCL into the layers of OMLS. In general, the intercalation can be done by using one of two approaches: (1) direct insertion of polymer chains from solution or the melt, or (2) insertion of a suitable monomer and subsequent polymerization. The present trial closely related to both, in which the polymerization was used to give a delamination and dispersion of OMLS and simultaneous plasticization of CA. THF solution of the sample was filtered through a membrane filter (pore size 0.2 μm) as pretreatment for GPC measurement, and OMLS layers were removed at that stage. Through GPC analysis, nonexistence of CL monomer within the obtained (CDA/OMLS)-g-PCL nanocomposites was confirmed, revealing the accomplishment of polymerization. GPC profiles of all the products showed higher molecular weight distributions than that of starting CA, which means that graft copolymerization to CA took place successfully,[23,26] even though OMLS was in-fed with CA.

It is known that CDA, although having the greatest thermoplasticity among the CAs, still lacks melt processability. However, when it was grafted with CL and introduced with oligoester side chains, CA, not limited to CDA, was easily converted into thermoplastic materials.[23,26] Thus, the present trial of preparing (CDA/OMLS)-g-PCL nanocomposites needed to fulfill this kind of thermoplasticization. Figure 1 presents an example of the results. Although the upper part of Fig. 1 confirms the above statement that CDA lacks sufficient thermoplasticity, the conversion to obtain complete thermoplastic material is shown to be achieved by this in situ polymerization (lower part of Fig. 1). This process was achieved in the present study in a series of nanocomposite preparations without exception.

Evidence of the intercalation, delamination, and/or exfoliation of the layered silicates during dispersion in the monomer, followed by in situ polymerization in the presence of CDA was obtained by measuring the XRD profile in the range of $2\theta = 1°–10°$ as shown in Figs. 2–4.

From Fig. 2, it can be seen that a small but insignificant expansion occurred in the highly purified montmorillonite (PGW) without organic modification during the monomer dispersion and polymerization process, and that almost no change was also observed for the synthetic fluoromica (ME-100). These results mean that effective organic modifications are required for layered silicates in order to obtain desirable nanocomposites.

In Fig. 3, how the organic modifications of layered silicates could enhance the expansion of the inter layer distance is shown. The mean layer spacing of the (001) plane (d_{001}) for the PGW and its organically modified sample (I-30T) are 1.05 nm (2θ = 8.44°) and 2.61 nm (2θ = 3.38°), respectively, revealing interlayer gallery expansion by this organic modification. This organically modified montmorillonite was synthesized by replacing Na^+ with octadecylammonium cation. The same type but larger gallery expansion was attained for synthetic fluoromicas ME-100 and MAE as is shown in Fig. 3b; that is, from 1.24 nm ($2\theta = 7.12°$) for ME-100 to 3.29 nm ($2\theta = 2.68°$) for MAE.

After the syntheses of nanocomposites, changes of the silicate interlayer distance (silicate–gallery spacing) (d_{001}) were also examined by XRD. Figure 4 shows the XRD patterns for OMLSs and corresponding nanocomposites prepared by the above-mentioned in situ polymerization, where the clays I-30T, SAN, MAE, SPN, MPE, Cloisite 30B, SEN, and MEE were used as OMLS. In Fig. 4a, for example, comparing with the characteristic peak of I-30T at $2\theta = 3.38°$ ($d_{001} = 2.61$ nm), the d_{001} peak of the corresponding nanocomposite, (CA/Cloisite 30B)-g-PCL, is found in a lower angle range of $2\theta = 2.60°$ (d_{001} = 3.40 nm), indicating that the gallery of montmorillonite is swollen by the intercalation of formed PCL and CA.

From Fig. 4, it is found that the degree of changes in the silicate–gallery spacing depends on the number of hydroxyl groups in each organomodifier. In the cases of non-OH modifiers, the change in silicate–gallery spacings is maintained within the range of intercalation, whereas there is a possibility that almost complete exfoliation is accomplished in the case of organomodifiers with two hydroxyl groups. The nanocomposites prepared from OMLS having one hydroxyl group lie between these extremes. Obtained nanocomposites were colored variously from pale yellow to dark brown. These colorations are likely to be caused by partial degeneration of organomodifiers or the nature of the layered silicate.

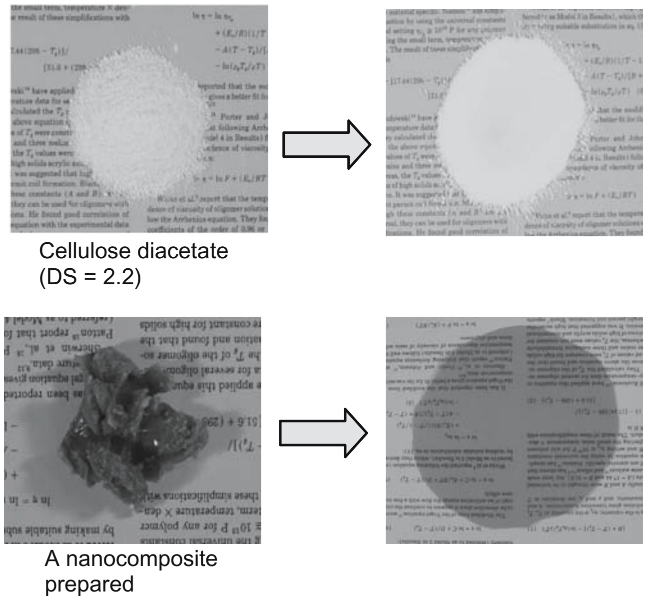

Fig. 1. Effect of the present nanocomposite formation on the thermoplasticization of the product. *Upper left*, cellulose diacetate (CDA; DS = 2.2) powder; *upper right*, CDA hot-pressed at 110°C under 15 MPa for 30 s; *lower left*, (CDA/SPN)-g-PCL nanocomposite; *lower right*, a sheet from the nanocomposite prepared by hot pressing at 110°C under 15 MPa for 30 s

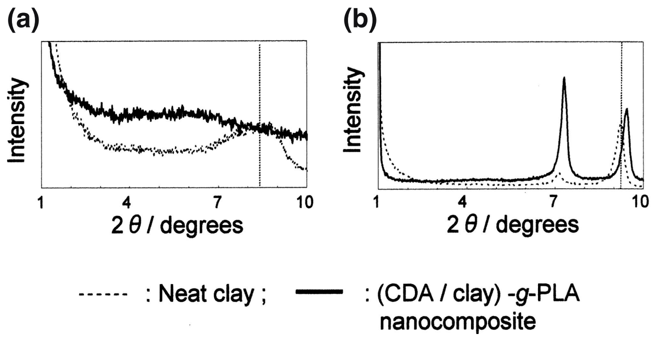

Fig. 2a,b. X-ray diffraction (XRD) profiles for **a** highly purified montmorillonite (PGW), and **b** synthetic fluoromica (ME-100) and their corresponding (CDA/clay)-g-PLA nanocomposite. The *vertical dashed lines* indicate the location of the silicate 001 reflection of the neat clay

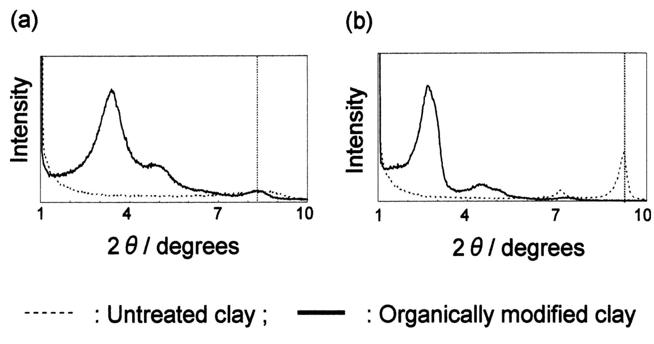

Fig. 3a,b. XRD profiles for **a** highly purified montmorillonites (PGW), and **b** synthetic fluoromicas (ME-100) and their organically modified examples (**a** I-30T, **b** MAE). The *vertical dashed lines* indicate the location of the silicate 001 reflection of the neat clay

Figure 5 shows the TEM micrographs taken in the edge direction (parallel to the film surface; the surface parallel direction is shown in each micrograph with solid line) for **a** (CDA/Cloisite 30B)-g-PCL, **b** (CDA/SPN)-g-PCL, and **c** (CDA/I-30T)-g-PCL nanocomposites (OMLS content = 5 wt%) in which dark moieties are the cross section of intercalated or exfoliated organoclay layers. In the case of **a**, the exfoliated silicate monolayers are found to be distributed randomly in the PCL-grafted CDA matrix. In the case of **b**, the SPN clays are found to exist in the form of aggregates composing of several stacked silicate layers, and their surfaces lay almost parallel to the film surface. That is, the stacked silicate layers show an arrangement in the direction of melt flow during the sheet formation. On the other hand, in the case of **c**, the I-30T OMLS does not disperse even after graft polymerization of CL. The clay silicates stacked together within the CDA-g-PCL matrix. These findings are in good keeping with those found in Fig. 4.

These lines of investigation are also well corroborated by the corresponding WAXS and SAXS patterns, as shown in Figs. 6 and 7. The X-ray beam was radiated on (CDA/SPN)-g-PCL and (CDA/Cloisite 30B)-g-PCL nanocomposite sheets in the through and edge directions, and WAXS and SAXS photographs were taken in which the through and edge directions were perpendicular and parallel to the film surface, respectively.

Figure 6 shows the WAXS and SAXS photographs for the (CDA/SPN)-g-PCL nanocomposite film in which the meridian for edge-view patterns is aligned in the film-thickness direction. Information concerning the interlayer spacing of the SPN layers can be obtained from the SAXS, whereas those including crystal structures of PCL are obtainable from WAXS.

In the edge-view pattern of WAXS, a strong and anisotropic intensity distribution[6,7] can be seen around the beam stop on the meridian, whereas the through-view pattern shows isotropic reflections. On the other hand, such a strong and anisotropic intensity distribution could not be seen for both view patterns of neat PCL (without OMLS).[28] These results suggest that such a strong intensity distribution is derived from the existence of the OMLS (SPN), which possesses an anisotropic shape in the film. Because the intensity maxima can be clearly observed along the meridian only for the edge-view pattern, the SPN layers appear to exist almost parallel to the film surface. Although the data thus obtained reveal the presence of SPN layers within the nanocomposite film, it was known that they made aggregates that were composed of a few numbers of stacked clays and matrix polymer. Its calculated interlayer spacing was 14.3 nm, which will be explained later, and the related TEM photograph is shown in Fig. 5.

The edge-view WAXS pattern shows a pair of stronger arc-like reflection, corresponding to the (110) plane of PCL crystallites on the equator, whereas the through-view pattern shows Debye-Scherrer rings, the latter of which suggests that the molecular axes are randomly oriented on the film plane. Concerning the former, it was found that the neat PCL did not exhibit such a preferred orientation of the crystallites. Thus, the former results mean that PCL molecules within the composite crystallize with their molecular chain axes (c-axis) oriented perpendicularly to the clay surface. The hot pressing temperature (110°C) is high enough that a preferred orientation may be developed under the influence of the clay. Because the polymerization of CL was initiated by the cocatalyst system of $SnEht_2$ and hydroxyl group within the modifier for the layered silicate, PCL crystallites were directly hooked on the clay surface, resulting in the aggregates by autonomous crystallization. In this case, PCL crystallization was restricted by the chemical bonding to the clay surface through the hydroxyl groups of organomodifiers, and also by the permitted interlayer distance between the clay walls. Thus, the crystallization was likely developed by a sort of transcrystallization, where the crystal growth was restricted in the confined space: such a crystallization mechanism was proposed in the composites of polybutene-1/polypropylene, poly(vinylidene fluoride)/nylon 11, and so forth.[29,30] This is hitherto an unknown observation for grafted cellulosic polymers, thus being highly interesting.

The yielded aggregated fillers composing (CDA/SPN)-g-PCL nanocomposite, thus, can gain enough mass to realize the orientation that the SPN layers appear to exist almost parallel to the film surface. This is in contrast to the cases of (CDA/Cloisite 30B)-g-PCL nanocomposite, where almost perfect exfoliation is accomplished as shown in Fig. 7.

Concerning the SAXS photographs in Fig. 6, the edge-view photograph exhibits four pairs of intensity maxima, being symmetrical around the beam stop, along the meridian. Such reflection, on the contrary, cannot be seen in the through-view pattern. Therefore, the molded film seems to have long-period structure units in its thickness direction. Spacings calculated are 14.3, 7.1, 4.7, and 3.6 nm from the smallest to the largest angles, respectively, which are in numerical ratio of 1 : 1/2 : 1/3 : 1/4 in this order, and are assigned to 001, 002, 003, and 004 reflections of PCL-grafted SPN (Fig. 6; edge-view of SAXS). The obtained long spacing of 14.3 nm is considered to be the result of the aggregation of grafted PCL, as described above, which results in a crystallization within the SPN interlayer and oriented perpendicular to its surface. In other words, the crystalline lamella of PCL shows stacking, the interval of which is restricted by the presence of the clay. On the other hand, there is possibility that intercalation of CDA would also occur taking a role in broadening the space.

It can be concluded from the above findings that complete exfoliation or delamination of clay layers does not

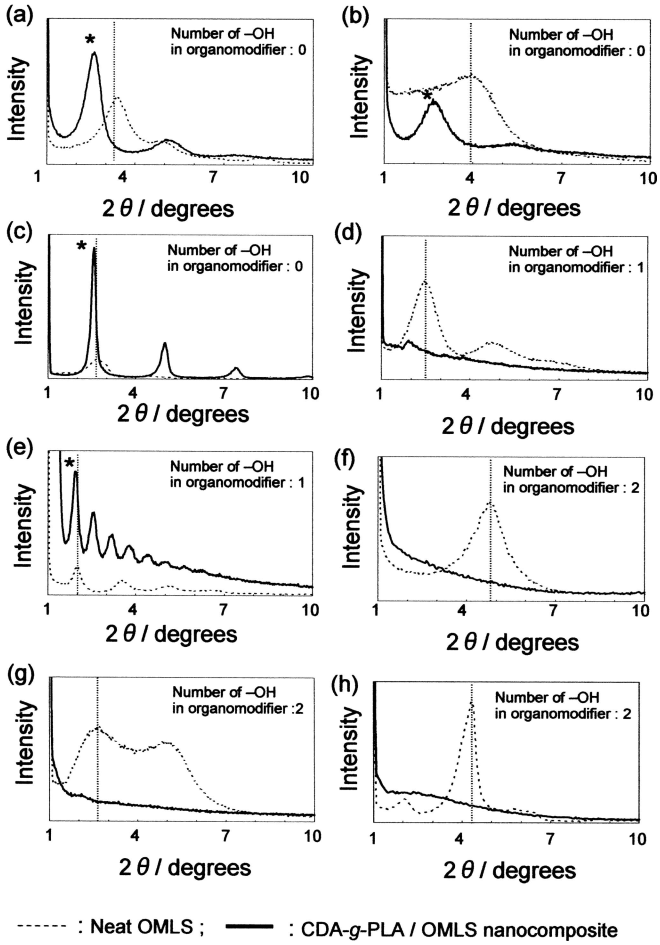

Fig. 4a–h. XRD profiles for organically modified layered silicates (OMLS) and (CDA/OMLS)-g-PCL nanocomposites. The *vertical dashed lines* indicate the location of the silicate 001 reflection of OMLSs. *Asterisks* indicate the (001) reflection of the nanocomposites. OMLSs used: **a** I-30T, **b** SAN, **c** MAE, **d** SPN, **e** MPE, **f** Cloisite 30B, **g** SEN, **h** MEE

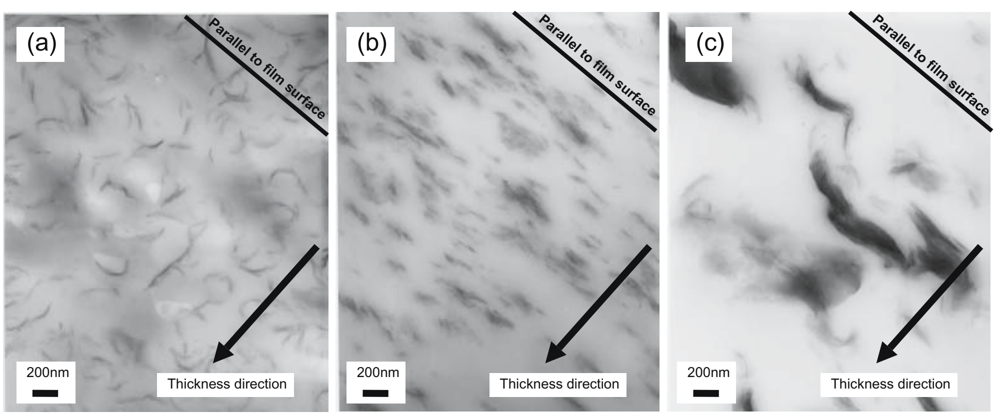

Fig. 5a–c. Transmission electron micrographs of **a** (CDA/Cloisite 30B)-g-PCL, **b** (CDA/SPN)-g-PCL, and **c** (CDA/I-30T)-g-PCL in situ graft polymerized nanocomposites (OMLS content 5%)

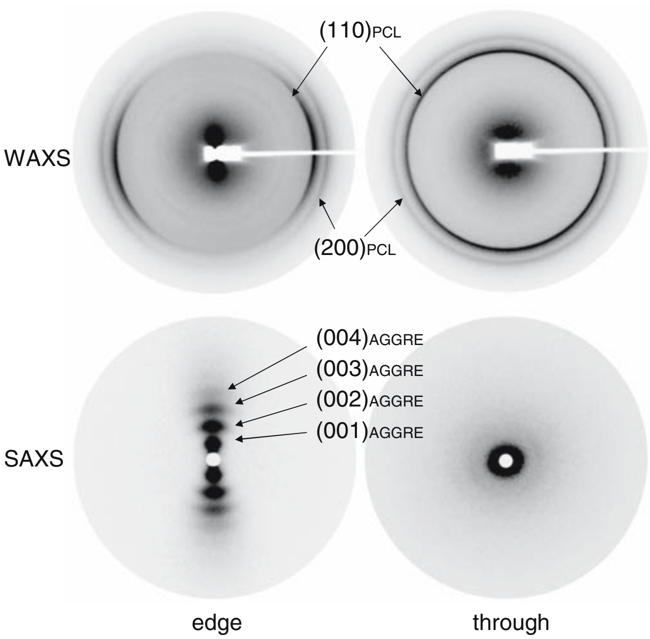

AGGRE, Aggregate of clay and PCL

Fig. 6. Wide-angle X-ray scattering (WAXS) and small-angle X-ray scattering (SAXS) patterns of (CDA/SPN)-g-PCL nanocomposite sheet (SPN 5 %)

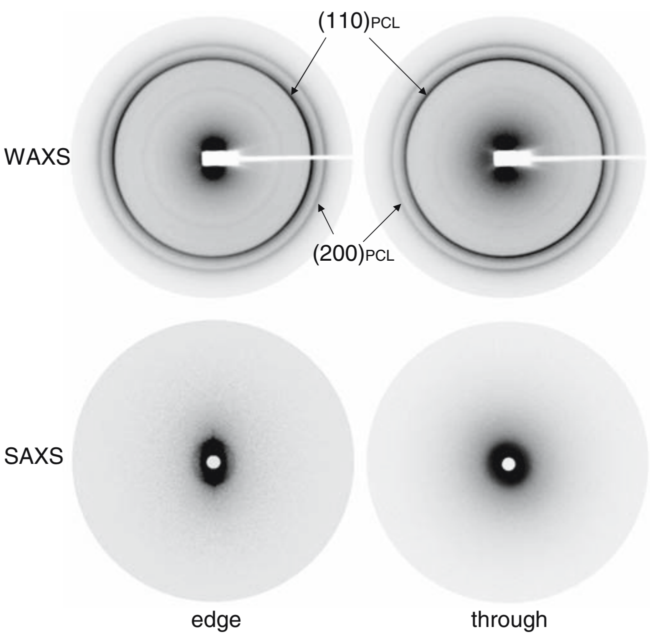

Fig. 7. WAXS and SAXS patterns of (CDA/Cloisite 30B)-g-PCL nanocomposite sheet (Cloisite 30B 5%)

take place in the (CDA/SPN)-g-PCL nanocomposite during the CL dispersion and its in situ grafting process, resulting in the aggregates. However, this aggregation causes its orientation to be parallel to the surface of the molded film, which is considered to impart an excellent water barrier and gas barrier properties to the nanocomposite products. As has been discussed, this parallel orientation of SPN to the surface is caused by its lamination, and an increase in the mass is due mainly to polymerization of CL on silicate layer surfaces. In this connection, the number of the silicate monolayers forming the aggregates was calculated from the TEM image (Fig. 5b), and found to be 4–10.

Figure 7 shows WAXS and SAXS photographs for the (CDA/Cloisite 30B)-g-PCL nanocomposite sheet, where the meridian of edge-view and through-view patterns is again aligned in the film-thickness direction. WAXS through-view and edge-view patterns in Fig. 7 show Debye-Scherrer rings, suggesting that the PCL molecular axes are randomly oriented on both the film planes. SAXS through-view pattern also shows an isotropic feature, whereas its edge-view shows some scattering of elliptical shape but still keeps the isotropic nature. These facts suggest that the Cloisite 30B silicate sheets are thin flat ones, randomly oriented in almost all the directions within the molded film. The above results are completely in keeping with those obtained in the corresponding XRD profile as shown in Fig. 4 and in TEM observations in Fig. 5.

From the above findings and arguments, it becomes apparent that, compared with the nanocomposite in which silicate layers are almost completely dispersed (exfoliated), the nanocomposite in which dispersion of silicate layers is not complete and several stacked silicate layer aggregates exist has higher functionality caused from their arrangement. Phenomena of this type have been found so far, for example, the Izod impact strength of Nylon-6/OMLS nanocomposites revealed the maximum value to be at an intermediate dispersion stage, whereas both the tensile strength and Young's modulus enlarged as the dispersion extent of OMLS was enhanced.[31]

Acknowledgments The synchrotron X-ray experiments were performed at the BL40XU beam line in SPring-8 facility, Harima, Japan, with the approval of the Japan Synchrotron Radiation Research Institute (Proposal number 2003B0436-NL2a-np). The authors thank Associate Prof. M. Wada and Dr. R. Hori of the University of Tokyo for their cooperation in the wide-angle and small-angle X-ray scattering measurements. The authors are also grateful to Emeritus Prof. K. Okamura for his critical reading of this article.

References

1. Messersmith PB, Giannelis EP (1994) Synthesis and characterization of layered silicate-epoxy nanocomposites. Chem Mater 6:1719–1725
2. Usuki A, Kawasumi M, Kojima Y, Okada A, Kurauti T, Kamigaito O (1993) Swelling behavior of montmorillonite cation exchanged for ω-amino acids by ε-caprolactam. J Mater Res 8:1174–1178
3. Kojima Y, Usuki A, Kawasumi M, Okada A, Kurauchi T, Kamigaito O, Kaji K (1994) Fine structure of nilon-6-clay hybrid. J Polym Sci Pol Phys 32:625–630
4. Messersmith PB, Giannelis EP (1995) Synthesis and barrier properties of poly(ε-caprolactone)-layered silicate nanocomposites. J Polym Sci Pol Chem 33:1047–1057
5. Gionnelis EP (1996) Polymer layered silicate nanocomposites. Adv Mater 8:29–35
6. Ogata N, Jimenez G, Kawai H, Ogihara T (1997) Structure and thermal/mechanical properties of poly(*l*-lactide)-clay blend. J Polym Sci Pol Phys 35:389–396

7. Jimenez G, Ogata N, Kawai H, Ogihara T (1997) Structure and thermal/mechanical properties of poly(ε-caprolactone)-clay blend. J Appl Polym Sci 64:2211–2220
8. LeBaron PC, Wang Z, Pinnavaia TJ (1999) Polymer-layered silicate nanocomposites: an overview. Appl Clay Sci 15:11–29
9. Okamoto M, Nam PH, Maiti P, Kotaka T, Hasegawa N, Usuki A (2001) A house of cards structure in polypropylene/clay nanocomposites under elongational flow. Nano Lett 1:295–298
10. Okamoto M, Nam PH, Maiti P, Kotaka T, Nakayama T, Ohshima M, Usuki A, Hasegawa N, Okamoto N (2001) Biaxial flow-induced alignment of silicate layers in polypropylene/clay nanocomposite foam. Nano Lett 1:503–505
11. Lee SR, Park HM, Lim H, Kang T, Li X, Cho WJ, Ha CS (2002) Microstructure, tensile properties, and biodegradation of aliphatic polyester/clay nanocomposites. Polymer 43:2495–2500
12. Shen Z, Simon GP, Chen Y-B (2002) Comparison of solution intercalation and melt intercalation of polymer–clay nanocomposites. Polymer 43:4251–4260
13. Ray SS, Okamoto K, Okamoto M (2003) Structure–property relationship in biodegradable poly(butylenes succinate)/layered silicate nanocomposites. Macromolecules 36:2355–2367
14. Pluta M, Galeski A, Alexandre M, Paul M-A, Dubois P (2002) Polylactide/montmorillonite nanocomposites and microcomposites prepared by melt blending: structure and some physical properties. J Appl Polym Sci 86:1497–1506
15. Ray SS, Yamada K, Okamoto M, Ueda K (2002) Polylactide layered silicate nanocomposite: a novel biodegradable material. Nano Lett 2:1093–1096
16. Yamada K, Ueda K, Ray SS, Okamoto M (2002) Preparation and properties of polylactide/layered silicate nanocomposite (in Japanese). Kobunshi Ronbunshu 59:760–766
17. Ray SS, Maiti P, Okamoto M, Yamada K, Ueda K (2002) New polylactide/layered silicate nanocomposites. 1. Preparation, characterization, and properties. Macromolecules 35:3104–3110
18. Ray SS, Maiti P, Yamada K, Okamoto M, Ogami A, Ueda K (2003) New polylactide/layered silicate nanocomposites. 3. High-performance biodegradable materials. Chem Mater 15:1456–1465
19. Paul M-A, Alexandre M, Degee P, Henrist C, Rulmont A, Dubois P (2003) New nanocomposite materials based on plasticized poly(L-lactide) and organo-modified montmorillonites: thermal and morphological study. Polymer 44:443–450
20. Ray SS, Yamada K, Okamoto M, Ueda K (2003) New polylactide-layered silicate nanocomposites. 2. Concurrent improvements of material properties, biodegradability and rheology. Polymer 44:857–866
21. Chang J-H, An YU, Cho D, Giannelis EP (2003) Poly(lactic acid) nanocomposites: comparison of their properties with montmorrillonite and synthetic mica (II). Polymer 44:3715–3720
22. Ray SS, Yamada K, Okamoto M, Ueda K (2003) Control of biodegradability of polylactide via nanocomposite technology. Macromol Mater Eng 288:203–208
23. Yoshioka M (2003) Biodegradable plastics from cellulose and lignocellulosics. In: Matsumura S, Steinbüchel A (eds) Biopolymers vol 9. Wiley, Weinheim, Germany, pp 201–235
24. Yoshioka M, Miyazaki T, Shiraishi N (1996) Plasticization of cellulose derivatives by reactive plasticizers I. Plasticization of cellulose acetate by kneading reaction using dibasic acid anhydrides and monoepoxides. Mokuzai Gakkaishi 42:406–416
25. Yoshioka M, Okajima K, Miyazaki T, Shiraishi N (2000) Plasticization of cellulose derivatives by reactive plasticizers II: characterization of plasticized cellulose acetates and their biodegradability. J Wood Sci 46:22–31
26. Yoshioka M, Hagiwara N, Shiraishi N (1999) Thermoplasticization of cellulose acetates by grafting of cyclic esters. Cellulose 6:193–212
27. Buchanan CM, Gardner RM, Komarck RJ (1993) Aerobic biodegradation of cellulose acetate. J Appl Polymer Sci 47:1709–1719
28. Bittiger B, Marchessault RH (1970) Crystal structure of poly-ε-caprolactone. Acta Crystallogr B 26:1923–1927
29. Takahashi T, Nishio Y, Mizuno H (1987) Crystallization behavior of polybutene-1 in the anisotropic system blended with polypropylene. J Appl Polym Sci 34:2757–2768
30. Li Y, Kaito A (2003) Crystallization and orientation behaviors of poly(vinylidene fluoride) in the oriented blend with nylon 11. Polymer 44:8167–8176
31. Chujo K (2002) On the Relation between the degree of delamination and the mechanical properties of polymer/clay nanocomposites (in Japanese). Seikei-Kakou 14:686–687